Layer-by-Layer Resistive Switching: Multistate Functionality due to Electric-Field-Induced Healing of Dead Layers

Jon-Olaf Krisponeit,[1,2,3,*] Bernd Damaschke,[2] Vasily Moshnyaga,[2] and Konrad Samwer[2]

[1]*Institute of Solid State Physics, University of Bremen, Otto-Hahn-Allee 1, 28359 Bremen, Germany*
[2]*I. Physikalisches Institut, Georg-August-Universität Göttingen, 37077 Göttingen, Germany*
[3]*MAPEX Center for Materials and Processes, University of Bremen, 28359 Bremen, Germany*

Materials exhibiting reversible resistive switching in electrical fields are highly demanded for functional elements in oxide electronics. In particular, multilevel switching effects allow for advanced applications like neuromorphic circuits. Here, we report a structurally driven switching mechanism involving the so-called "dead" layers of perovskite manganite surfaces. Forming a tunnel barrier whose thickness can be changed in monolayer steps by electrical fields, the switching effect exhibits well-defined and robust resistive states.

Resistance switching effects driven by electric fields are raising hope for novel multistate memory applications and, mimicking biological synapses, for advances in neuromorphic computing [1,2]. Functional oxides meet their demand for nonbinary resistance changes covering several orders of magnitude by providing mechanisms as diverse as displacive effects [3], ferroelectric domain switching [4], and the tuning of Schottky barriers [5]. These approaches rely on the accurate fabrication of oxide heterostructures. Avoiding such complexity, we demonstrate here that multistate functionality can be obtained already in a single material. Perovskite manganites are known to exhibit so-called dead layers [6–10] forming at interfaces and at the free surface. We show that such dead layers can indeed play a most active role: Being switchable in a layer-by-layer fashion between two intrinsically well-defined resistance states, they might pave the way to novel concepts for robust switching devices as stepwise tunable tunnel barriers.

The resistive switching behavior at the free surface of an epitaxial manganite thin film grown on MgO(100) has been analyzed by conductive atomic force microscopy (CAFM). The film with nominal composition $La_{0.85}Sr_{0.15}MnO_3$ was grown by means of a metalorganic aerosol deposition technique [11]. The precursors, acetylacetonates of La, Sr, and Mn, were solved in dimethylforamide and sprayed onto the heated substrate ($\sim900\,°C$ in ambient atmosphere) by compressed air. The molar ratio of precursors in the solution was tuned to obtain the necessary film stoichiometry with Sr-doping level, $x \approx 0.15$, as was empirically calibrated by means of x-ray diffraction and energy dispersive x-ray microanalysis. According to the x-ray diffraction, the film shows an out-of-plane epitaxy on MgO with c-axis lattice constant $c = 0.3899$ nm, which is very close to the bulk LSMO value for $x = 0.15$–0.17 [12], indicating a strain-free state of the film. A thickness of $d \approx 60$ nm was estimated from the used precursor amount, calibrated from similar LSMO films by using small-angle x-ray reflectivity. Resistance measurements reveal an insulator-metal transition at $T_{MI} = 290$ K and a metalliclike behavior $dR/dT > 0$ at low temperatures with relatively high residual resistivity $\rho(10K) \approx 5 \times 10^{-4}$ Ohm cm (see Supplemental Material [13]) possibly due to a phase separation as the chosen composition is close to the MI phase boundary in the phase diagram of LSMO, $x = 0.175$ [12].

All switching experiments were carried out at room temperature with an Omicron VT-AFM under ultrahigh vacuum conditions (base pressure $< 3 \times 10^{-10}$ mbar). Commercial probes from MikroMasch with a spring constant of 0.15 N/m and a Pt coating were used for CAFM measurements. Note that due to the coating the tip radius is enlarged, leading to reduced topographic resolution in comparison with standard AFM probes. Measurements were recorded at vertical force set points ≤ 5 nN, all current maps shown were recorded at a positive tip bias of 0.1 V. Scanning the sample surface with a conductively coated tip, CAFM enables local switching experiments on a nanometer scale as well as the simultaneous recording of topography and current maps. It has hence proven indispensable for microscopic investigations of memristive effects [14–19]. As reported in our previous studies on comparable epitaxial [14,19] and nanocolumnar [18] manganite thin films, the LSMO surface exhibits an initial state of a very high resistance (HRS), which can be switched to a low resistive state (LRS) by application of a positive electric pulse above a critical threshold voltage to the tip. The HRS can be restored again by a voltage pulse of the reversed (negative) polarity. A current map of conductive surface regions created at the initially insulating surface by positive voltage pulses is given in Fig. 1(a).
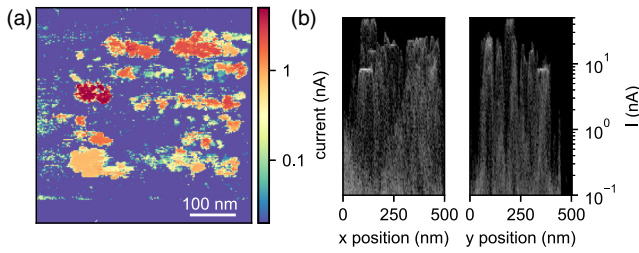
FIG. 1. Metallic regions created by electric pulses at the initially insulating surface. (a) Current map recorded at 0.1 V showing the spatial distribution of conductance at the surface. (b) Distribution of current values with respect to their x and y position, visualizing regions of homogeneous conductance as horizontal lines.

The domain distribution was obtained by 64 positive voltage pulses, applied in a regular square pattern with increasing pulse voltages, ranging from $+3$ V to $+6.5$ V, from bottom to top and pulse durations increasing from 1 ms to 3 s from left to right, see also Ref. [14] for comparison. The irregular lateral shape of conducting domains originates from their cascadelike growth dynamics dominated by domain wall pinning at defects and the surface morphology [19].

Interestingly, beyond the previously reported manganite switching characteristics, we observe here the formation of apparently discrete conductance levels on a microscopic scale: Although the CAFM tip was at rest during the voltage pulses, the regions of homogeneous conductance were extended to significantly larger dimensions (up to 100 nm) than the actual electrical contact (few nanometers in diameter). This observation not only excludes a filamentary process for the given case, but the existence of sharp domain boundaries furthermore also implies an abrupt transition proceeding through the material instead of a gradual change. For further analysis, the frequency of the measured conductance values was visualized depending on the x and y positions of the tip [Fig. 1(b)]. In these intensity maps, the discrete conductance values can be clearly discerned as horizontal lines. These values scatter seemingly arbitrarily, predominantly in the upper part of the instrumental current range (50 nA) and no correlation between current and sample topography was found.

For investigations of the reversed switching direction from LRS to HRS, another sample region has been set to the metallic surface state by several fast scans (1000 nm) under a positive electrical tip bias of 6 V. By using this technique instead of prolonged pulses with the cantilever resting at a single site, we could avoid thermal damaging of the surface impending from local joule heating in the LRS. As confirmed via simultaneously recorded current maps, the low resistive state has been successfully created on the entire scan area. Next, voltage pulses of reversed (negative) polarity have been applied at four cantilever positions, whereupon two extended areas of increased resistivity have
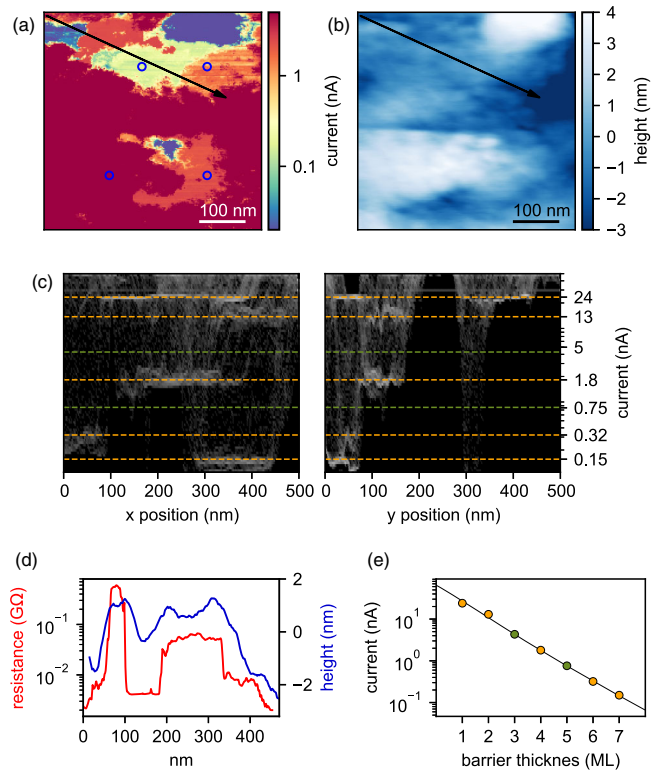

FIG. 2. Conductance and topography regions switched from LRS to HRS. (a) Current map recorded at $U = 0.1$ V. After switching to LRS (red environment), negative voltage pulses have been applied at the locations indicated by circles. (b) Corresponding topography image. The correlation between contact resistance (red) and height (blue) is illustrated by profiles along the indicated path (d). (c) Distribution of current values occurring in dependence of the x and y locations as intensity map. Identified logarithmically spaced current values are shown in orange, missing levels are indicated in green. (e) Current in dependence of the ascribed tunnel barrier thickness with fit curve according to MIM model.

emerged: one around the lower right pulse position and one including both upper pulse positions in Fig. 2(a). No successful switching was observed at the lower left pulse position. As is obvious from the current map, both areas comprise subregions of homogeneous conductivity. Furthermore, though disjunct, each area contains one subregion belonging to the same current level (≈ 25 nA).

Comparison with the topography data [Fig. 2(b)], as further illustrated by line profiles of height and resistance [Fig. 2(d)], reveals a remarkable correlation between the sample height and the magnitude of the discrete resistance levels. Regions of lower (higher) resistance are found primarily in shallow (protruding) regions, respectively. Taking into account that the vertical length scale spans only few lattice constants, we hence claim that the discrete current values stem from insulating barriers with thicknesses of integer numbers of atomic layers. Contrasting the initial switching process discussed above, the intensity

maps [Fig. 2(c)] now suggest a nonrandom, logarithmic spacing of the possible current values, indicating the insulating barrier to act as a tunnel barrier. We therefore ascribe the HRS levels to the existence of so-called dead layers. These regions, where magnetic and electric properties deviate from the bulk, are well documented to occur on manganite films at interfaces as well as at their free surfaces and may result in a tunnel barrier. Reports agree in estimating typical dead layer thicknesses of about 3 to 4 nm for LSMO films under different strain influences arising from a variety of chosen substrates [6–10]. While the exact physical origin for the formation of dead layers is still under discussion, the symmetry break at interfaces and variations in the oxygen content have been identified as key factors. Recent investigations on LSMO elucidated the interfacial loss of inversion symmetry to lift the degeneracy of the $3d - e_g$ orbitals, resulting in a preferential occupation of the out-of-plane $3z^2 - r^2$ orbitals and the emergence of a C-type antiferromagnetic layer with a thickness of ≈ 2.4 nm [20,21].

Our results imply that such a dead layer can indeed be "healed" by the application of positive voltage pulses, and the dead HRS state is forming again under reversed polarity both proceeding in a layer-by-layer fashion. A simplified sketch is shown in Fig. 3(a). At low temperatures, the half-metallic bulk LSMO exhibits an exchange splitting of the conduction band formed by the $3d - e_g$ states. At room temperature, although close to T_{MI}, it still shows a considerably high conductivity according to macroscopic measurements (see Supplemental Material [13])—incompatible with the highly insulating initial state found by CAFM. Hence, at the surface, we assume a dead layer with strong electronic correlations and a gap opening

between an upper and lower Hubbard band. Because of this gap, an intrinsic tunnel barrier is formed between the bulk LSMO and the top electrode, i.e., the Pt-coated AFM tip. The width of this barrier and therewith the tunneling conductance can be modified by electric fields. Note that in this scenario only two well-defined intrinsic resistive states are involved and the observed multitude of "device" resistance levels originates solely from the varying number of layers forming the insulating barrier at the surface. This picture contains strong conceptual similarities with adaptive states arising from switchable domain boundaries in multiferroic materials [22,23] and the switching of ferroelectric and multiferroic tunnel junctions [4,24,25]. The combination of the LSMO bulk, which is also often utilized as a half-metallic lead material in the latter case, and the functional surface layer could be regarded as an "intrinsic heterostructure" showing related physical phenomena. However, requiring a precise description of the complex interplay with the t_{2g} states, the $O2p$ band and structural correlations, the derivation of a detailed microscopic model is obviously beyond the scope of this study. Interestingly, Shen *et al.* very recently proposed a possible magneto-structural mechanism for the switching of dead layers—in that case resulting in a suppression of spin-polarized transport in half-metallic $La_{0.7}Ca_{0.3}MnO_3$ [26].

In their recent work, Norpoth *et al.* [27] provided evidence that in the case of $Pr_{0.7}Ca_{0.3}MnO_3$ resistive switching processes can actually involve a combination of structural transitions and oxygen vacancy migration. In our case, the results indicate the structural-electronic transition of LSMO dead layers to act as the fundamental switching step. This is clearly a distinct mechanism, which acts independently at the surface of the sample. Diffusive switching processes affecting larger sample fractions can yet be stimulated by, e.g., high current densities and joule heating due to the switched surface. For future applications, however, the opportunity to exploit an abrupt transition between two well-defined states might promise extraordinary device robustness on small length scales.

Let us now review the phenomenological model of surface dead layers and consider the discrete current values to reflect tunnel barriers of integer monolayer thickness. Therefore, the resulting metal-insulator-metal (MIM) architecture was treated within tunneling theory. For a proof of the model, we tentatively assigned an increasing layer thickness of perovskite monolayers to the current values in descending order. Five current values could be reliably identified in the corresponding intensity maps [Fig. 2(d)]. In addition, the maps suggest only logarithmically spaced current values to be allowed. We believe that two of these possible current levels have not been realized in the experiment, which have therefore been included as interpolated values. As illustrated in Fig. 2(e), the current values decrease approximately exponentially with the assumed layer thickness, confirming the existence of a tunnel barrier.
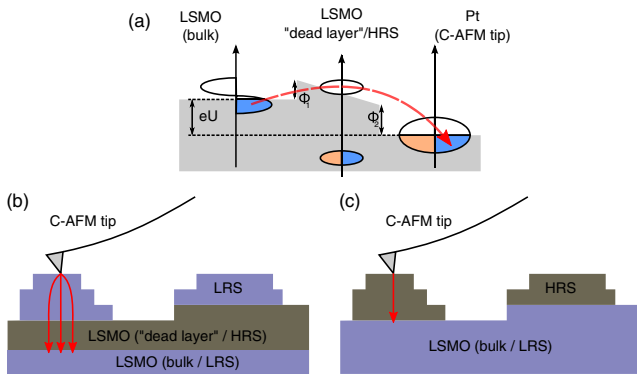

FIG. 3. Schematic band picture of the intrinsic tunnel barrier and geometrical contact model of the regions switched in CAFM. (a) The bulk of the LSMO and the Pt-coated AFM tip are separated by an insulating tunnel barrier. (b) Switching to LRS creates metallic regions at the surface, which act as broadened electrode to the underlying barrier. (c) Applying negative voltage pulses at a fully LRS-switched sample creates insulating layers of integer monolayer thicknesses at the surface, giving rise of the logarithmically stepwise scaling of the current values.

One has to keep in mind, however, that no direct determination of the barrier thickness is possible from the experiment and that the minimal barrier thickness of one monolayer chosen here is arbitrary. The same exponential behavior would be observed for an offset in the ascribed layer thickness. Barriers of even higher thickness are difficult to be observed in our experiments, because the tunneling current would lie at or beneath the instruments noise level. Yet, the investigated range of 7 ML (≈ 2.7 nm) agrees well with the typical thicknesses of dead layers estimated in the aforementioned studies.

The height of the tunnel barrier at the hidden interface, ϕ_I, has been estimated according to the formula derived by Simmons for MIM architectures [28,29]. In our case, a satisfactory fit result [see Fig. 2(e)] could be obtained only for the case of high voltages, i.e., where $eV > \phi_{II}$, with ϕ_{II} being the barrier height between the LSMO surface and the Pt AFM tip [Fig. 3(a)]. The current is given by

$$I = \frac{A\kappa}{\phi_I(z+z_0)^2}\left(e^{-\lambda(z+z_0)\phi_I^{3/2}} - be^{-\lambda(z+z_0)\phi_I^{3/2}b}\right). \quad (1)$$

Here, $\kappa = (e^3U^2/8\pi^2\hbar)$ and $\lambda = (2\beta\sqrt{2m}/eU\hbar)$, depending only on the applied tip voltage, are known constant, where $\beta = \frac{23}{24}$ for a triangular barrier shape [29] and $b = \sqrt{1 + 2eU/\phi_I}$. For the effective mass of the charge carriers in LSMO the value estimated by Okuda et al. of $m \approx 2.5m_0$ (Ref. [30]) was used. U is the bias voltage applied to the cantilever tip. Considering the existence of a minimal barrier thickness, an additional offset z_0 has been taken into account for z. Three physical fitting parameters have been derived: The barrier height ϕ_I, the minimum barrier thickness z_0 and the electrical contact area A. The latter two parameters are strongly correlated and cannot be reliably determined from the fitting procedure. Nevertheless, we obtained reasonable values for $A \approx 2.0$ nm^2 (see Ref. [14] for an estimation) and $z_0 \approx 1.3$ nm, further validating the model. The barrier height has been determined as $\phi_I = 46$ meV. Because of the uncertainties regarding A and z_0, the limited data available, and, first of all, the not precisely known effective mass, we have to consider this value as a rough estimate but trust in ϕ_I being below 60 meV. Thus, the observed exponential thickness dependence of the current and a convincing fit by the Simmons model evidence a tunneling behavior in our CAFM measurements.

Being remarkably small, this barrier height between bulk LSMO and the dead layer might be indicative for band bending effects but also for a Fermi level pinning closely below the conduction band inside the dead layer. This behavior would not constitute a contradiction to previous results, as significant Fermi level pinning has been excluded only for bulk LSMO which lacks the tendency for intrinsic electronic phase separation. While the minimal barrier thickness cannot be accurately determined from the given fit and some thickness values might

be allowed yet unrealized in the presented experiments, it is yet remarkable that the obtained value of 1.3 nm is in perfect agreement with the results of Valencia et al. of a 2–4 ML thick very robust C-type antiferromagnetic layer at LSMO interfaces [21].

Finally, we must address the question OF why logarithmically spaced current values have been observed only for the switching direction from LRS to HRS and not vice versa, where nevertheless patches of homogeneous conductance were found. Indeed, a careful investigation based on the contact geometry provides a phenomenological understanding of this behavior: The initial state of the sample has to be regarded as sketched in Fig. 3(b), with the dead layer extending to an intrinsic, characteristic depth. It is natural to assume the energetical preference of a flat interface between bulk and dead layer, hence small surface corrugations lead to locally increased barrier thicknesses. Considering the switching from HRS to LRS to be initiated at the tip—where the electric field strength is maximal— switched metallic regions grow into the sample. Depending on the pulse strength, duration and pinning processes at defects and, in particular, the surface morphology, a metallic region of variable size grows atop the dead layer. Note that in a previous study on similar manganite films we have demonstrated the importance of domain wall pinning and depinning effects in the evolution of metallic regions as reflected in the occurrence of avalanchelike dynamics [19].

As a consequence, a MIM structure evolves with an effectively enlarged top electrode of random size. The observed current values depend on its lateral dimensions as well as on the reduced dead layer thickness remaining underneath. This picture therefore meets the observed randomness and the generally higher current values as observed in the experiment. On the other hand, having switched the entire surface region to the LRS it is most intuitive to assume the switching process to initiate at the topmost layers again proceeding layerwise into the sample [Fig. 3(c)]. Now, only the CAFM tip acts as top electrode— probing the insulating layer thickness with a constant tip-to-sample contact area and hence depicting the logarithmically scaled current values. Moreover, the bulk LSMO is at all times remaining in a LRS in comparison to the highly insulating dead layer. Because of a very large area, $\approx$few mm^2, it contributes a much lower resistance even at room temperature, $T \approx T_{\mathrm{MI}}$, and despite the globally insulating state according to the $R(T)$ dependence.

To conclude, we have presented evidence for a layer-by-layer proceeding resistive switching. For the underlying physical mechanism, the existence of dead layers acting as tunnel barriers appears to be a crucial factor. The layerwise appearance further suggests for resistive switching at the LSMO surface an electro- or magnetostructural transition rather than a diffusive mechanism. From an applicational perspective, the existence of two inherent, well-defined resistivity states and the demonstrated possibility to actively

control them on a monolayer scale might trigger novel approaches to resistive switching devices featuring improved device lifetimes due to the robustness against chemical and structural degradation of the structural mechanism. The new, stepwise switching mode provides a solid multistate functionality as desired for advances in oxide electronics and neuromorphic computing architectures.

---

*krisponeit@ifp.uni-bremen.de

[1] J. J. Yang, D. B. Strukov, and D. R. Stewart, Nat. Nanotechnol. **8**, 13 (2013).

[2] R. Waser and M. Aono, Nat. Mater. **6**, 833 (2007).

[3] J. J. Yang, M. D. Pickett, X. Li, D. A. A. Ohlberg, D. R. Stewart, and R. S. Williams, Nat. Nanotechnol. **3**, 429 (2008).

[4] A. Chanthbouala, V. Garcia, R. O. Cherifi, K. Bouzehouane, S. Fusil, X. Moya, S. Xavier, H. Yamada, C. Deranlot, N. D. Mathur, M. Bibes, A. Barthélémy, and J. Grollier, Nat. Mater. **11**, 860 (2012).

[5] A. A. Bessonov, M. N. Kirikova, D. I. Petukhov, M. Allen, T. Ryhänen, and M. J. A. Bailey, Nat. Mater. **14**, 199 (2015).

[6] L. Jin, C.-L. Jia, I. Lindfors-Vrejoiu, X. Zhong, H. Du, and R. E. DuninBorkowski, Adv. Mater. Interfaces **3**, 1600414 (2016).

[7] R. P. Borges, W. Guichard, J. G. Lunney, J. M. D. Coey, and F. Ott, J. Appl. Phys. **89**, 3868 (2001).

[8] M. Huijben, L. W. Martin, Y. H. Chu, M. B. Holcomb, P. Yu, G. Rijnders, D. H. A. Blank, and R. Ramesh, Phys. Rev. B **78**, 094413 (2008).

[9] J. Z. Sun, D. W. Abraham, R. A. Rao, and C. B. Eom, Appl. Phys. Lett. **74**, 3017 (1999).

[10] B. Kim, D. Kwon, T. Yajima, C. Bell, Y. Hikita, B. G. Kim, and H. Y. Hwang, Appl. Phys. Lett. **99**, 092513 (2011).

[11] V. Moshnyaga, I. Khoroshun, A. Sidorenko, P. Petrenko, A. Weidinger, M. Zeitler, B. Rauschenbach, R. Tidecks, and K. Samwer, Appl. Phys. Lett. **74**, 2842 (1999).

[12] A. Urushibara, Y. Moritomo, T. Arima, A. Asamitsu, G. Kido, and Y. Tokura, Phys. Rev. B **51**, 14103 (1995).

[13] See Supplemental Material at http://link.aps.org/supplemental/10.1103/PhysRevLett.122.136801 for temperature dependent resistivity data.

[14] J.-O. Krisponeit, C. Kalkert, B. Damaschke, V. Moshnyaga, and K. Samwer, Phys. Rev. B **82**, 144440 (2010).

[15] X. Chen, N. Wu, J. Strozier, and A. Ignatiev, Appl. Phys. Lett. **89**, 063507 (2006).

[16] C. Moreno, C. Munuera, S. Valencia, F. Kronast, X. Obradors, and C. Ocal, Nano Lett. **10**, 3828 (2010).

[17] R. Münstermann, J. J. Yang, J. P. Strachan, G. Medeiros-Ribeiro, R. Dittmann, and R. Waser, Phys. Status Solidi RRL **4**, 16 (2010).

[18] C. Kalkert, J.-O. Krisponeit, M. Esseling, O. I. Lebedev, V. Moshnyaga, B. Damaschke, G. van Tendeloo, and K. Samwer, Appl. Phys. Lett. **99**, 132512 (2011).

[19] J.-O. Krisponeit, C. Kalkert, B. Damaschke, V. Moshnyaga, and K. Samwer, Phys. Rev. B **87**, 121103(R) (2013).

[20] D. Pesquera, G. Herranz, A. Barla, E. Pellegrin, F. Bondino, E. Magnano, F. Sánchez, and J. Fontcuberta, Nat. Commun. **3**, 1189 (2012).

[21] S. Valencia, L. Peña, Z. Konstantinovic, L. I. Balcells, R. Galceran, D. Schmitz, F. Sandiumenge, M. Casanove, and B. Martínez, J. Phys. Condens. Matter **26**, 166001 (2014).

[22] E. K. H. Salje, ChemPhysChem **11**, 940 (2010).

[23] D. D. Viehland and E. K. H. Salje, Adv. Phys. **63**, 267 (2014).

[24] D. Pantel, S. Goetze, D. Hesse, and M. Alexe, Nat. Mater. **11**, 289 (2012).

[25] M. Gajek, M. Bibes, S. Fusil, K. Bouzehouane, J. Fontcuberta, A. Barthélémy, and A. Fert, Nat. Mater. **6**, 296 (2007).

[26] X. Shen, T. J. Pennycook, D. Hernandez-Martin, A. Pérez, Y. S. Puzyrev, Y. Liu, S. G. E. te Velthuis, J. W. Freeland, P. Shafer, C. Zhu, M. Varela, C. Leon, Z. Sefrioui, J. Santamaria, and S. T. Pantelides, Adv. Mater. Interfaces **3**, 1600086 (2016).

[27] J. Norpoth, S. Mildner, M. Scherff, J. Hoffmann, and C. Jooss, Nanoscale **6**, 9852 (2014).

[28] J. G. Simmons, J. Appl. Phys. **34**, 238 (1963).

[29] J. G. Simmons, J. Appl. Phys. **34**, 1793 (1963).

[30] T. Okuda, A. Asamitsu, Y. Tomioka, T. Kimura, Y. Taguchi, and Y. Tokura, Phys. Rev. Lett. **81**, 3203 (1998).